



CHORUS

This is the accepted manuscript made available via CHORUS. The article has been published as:

Dirac donor states controlled by magnetic field in gapless and gapped graphene

Jia-Lin Zhu, Songyang Sun, and Ning Yang

Phys. Rev. B **85**, 035429 — Published 19 January 2012

DOI: [10.1103/PhysRevB.85.035429](https://doi.org/10.1103/PhysRevB.85.035429)

Dirac electron controlled by Coulomb and magnetic fields in gapless/gapped graphene

Jia-Lin Zhu* and Songyang Sun

Department of Physics, Tsinghua University, Beijing 100084, China

Ning Yang

Institute of Applied Physics and Computational Mathematics, P.O. Box 8009(28), 100088 Beijing, China

(Dated: November 18, 2011)

In this paper, the exact solutions of Dirac electronic states of graphene in Coulomb and magnetic fields are acquired. The Coulomb field not only causes the splitting of Landau levels in gapless graphene but also leads to the variation of the energy level ordering in gapped graphene. The dependence of the binding energies on the gap and the magnetic field is discussed. Furthermore, the valley degree of freedom and the valley splitting spacing can be controlled by the Coulomb and magnetic fields in gapped graphene. The inter-valley mixing of graphene is estimated and calculated in the direct sum spaces of the two valleys. The results obtained help to understand the behaviors of the planar Dirac electron in electromagnetic fields and can be applied to the controlling of electron's behaviors in graphene.

PACS numbers: 73.22.Pr, 73.20.Hb

I. INTRODUCTION

The discovery of graphene¹⁻⁴ has provided a platform to study the planar Dirac particles in quantum electrodynamics(QED). Due to its linear dispersion at the two inequivalent points K and K' of the Brillouin zone,⁵ the electronic structure of graphene in the vicinity of the valley $K(K')$ is described by Dirac equation with the wave functions at K and K' related by time-reversal symmetry.⁴ The electron in graphene is usually considered massless and recent experiments can introduce an adjustable gap (rest mass) to graphene systems, which is crucial for the application in making devices.⁶⁻⁸

As doping plays a key role in the conventional semiconductor physics, impurity problem in graphene has come into researchers' attention.^{9-11,13-19} A simple and practical model is the long-range Coulomb impurity in graphene. The effects of the Coulomb impurities on the transport properties,¹⁰⁻¹² the bound (quasibound) states of the Coulomb impurity^{13,14} and its screening effects¹⁵⁻¹⁸ have been investigated systematically by both the tight-binding model on the lattice and the two dimensional (2D) Dirac equation. The Coulomb attractive impurity in graphene mimics heavy atoms in QED¹⁹ and presents an accessible way to investigate the fundamental quantum relativistic phenomenon of QED, such as atomic collapse and the supercritical nuclei.^{15,16} Under uniform magnetic field, the well-known Landau levels (LLs) in graphene are also relativistic, square root dependent on the magnetic field and the Landau index, which are confirmed by both the quantum Hall effect² and the Landau level spectroscopy.^{20,21} Therefore, it is a new way to study and control the Dirac particles of 2D QED in electromagnetic fields by investigating the behaviors of the electron in either valley of graphene. The planar Dirac equation can be solved analytically in either Coulomb or magnetic field, but its full spectra in Coulomb and magnetic fields haven't been ob-

tained exactly since the problem is beyond the analytical solution.^{22,23} It is important to realize that the difference between the graphene systems and 2D QED lies in that the valley degree of freedom has to be taken into account when the valley degeneracy of graphene is broken. The LLs are valley degenerate for low-lying states when the magnetic field is not very high ($< 10T$), but Zhang et al observed experimentally the splitting of the K and K' valleys at high magnetic fields ($> 11T$).²⁴ Theoretically, a number of mechanisms are proposed to lead to the valley splitting, such as disorder,^{25,26} the effect of the trigonal warping,²⁷ graphene ring structures²⁸ and electron-electron interactions.^{29,30} These researches inspire us to explore the valley splitting of gapped graphene in Coulomb and magnetic fields. To systematically investigate the planar Dirac electron in electromagnetic fields, in this paper we generalize the series expansion method³¹ to the exact numerical solution of the Dirac electron confined by Coulomb and magnetic fields in graphene. On one hand, based on the exact solution, we study how the spectra of the planar Dirac electron of QED evolve in Coulomb and magnetic fields and the method given in this paper may be generalized to other complex systems of QED; on the other hand, in graphene we further investigate the effect of the Coulomb and magnetic fields on the valley splitting and estimate the inter-valley mixing caused by the Coulomb field in the direct sum spaces of the K and K' valleys.

The paper is organized as follows: In Sec.II, we present the Hamiltonian model and the calculation method of series expansion. In Sec.III, we systematically investigate the evolution of the spectra of the massless and massive Dirac electron in Coulomb and magnetic fields in valley K . In Sec.IV, we further calculate the valley splitting and estimate the magnitude of the inter-valley mixing in graphene, followed by a conclusion in Sec.V.

II. HAMILTONIAN MODEL AND CALCULATION METHOD

In the framework of the effective mass theory, we first suppose the Coulomb potential doesn't mix K and K' ^{14,15} so that we can solve the Dirac equation in each valley separately and then in Sec.IV we will discuss the inter-valley mixing caused by the Coulomb field in the direct sum spaces of the two valleys. In gapless graphene, the screening which results from the electron-electron interaction, preserves the shape of the Coulomb field and simply reduces its strength^{13,14} while the screening is complicated in gapped graphene.¹³ In the following, we assume that the shape of the impurity potential obeys the Coulomb law in both gapless and gapped graphene.^{13,23} Then the Hamiltonian for the Dirac electron confined by Coulomb and magnetic fields in the K and K' valleys is written as

$$\hat{H}^\tau = v_F \sigma_x (P_x + eA_x) + \tau v_F \sigma_y (P_y + eA_y) + m v_F^2 \sigma_z - \frac{v_F \alpha}{r} \quad (1)$$

where $v_F \approx 10^6 m/s$ is the Fermi velocity, \vec{P} is the momentum operator, \vec{A} is the magnetic vector potential, m is the mass, σ_x, σ_y and σ_z are the 2×2 Pauli matrices, $\tau = 1(-1)$ labels valley $K(K')$. We adopt the gauge $\vec{A} = \frac{1}{2} B r \vec{e}_\theta$ and separate the radial and azimuthal parts of the two-component wave function the upper and lower components of which represent the envelope functions for the A and B sublattices in graphene. We label φ and χ as the radial parts of the upper and lower components. The wave functions for K and K' are $\Psi^K = \frac{1}{\sqrt{r}} (\varphi^K e^{i l \theta}, i \chi^K e^{i(l+1)\theta})^T$ and $\Psi^{K'} = \frac{1}{\sqrt{r}} (i \varphi^{K'} e^{i(l+1)\theta}, \chi^{K'} e^{i l \theta})^T$, respectively, where i is the imaginary unit. For convenience, we set the scales of the length and energy as $a_0 = \sqrt{\frac{\hbar}{e B_0}}$ and $E_0 = \frac{\hbar v_F}{a_0}$ where $B_0 = 1 T$. Thus, $a_0 = 25.656 nm$ and $E_0 = 25.656 meV$. $\alpha = \frac{Z e^2}{4 \pi \epsilon \epsilon_0 \hbar v_F}$ is dimensionless and is lower or near 0.5 for typical substrate materials in experiments.^{9,13,17} Then we get the following radial functions from $\hat{H}^\tau \Psi^\tau = E^\tau \Psi^\tau$

$$\begin{cases} \left(\frac{d}{dr} + \frac{i}{r} + \frac{1}{2} B r \right) \chi^K = (E - M + \frac{\alpha}{r}) \varphi^K \\ \left(\frac{d}{dr} - \frac{i}{r} - \frac{1}{2} B r \right) \varphi^K = -(E + M + \frac{\alpha}{r}) \chi^K \end{cases} \quad (2)$$

$$\begin{cases} \left(\frac{d}{dr} - \frac{i}{r} - \frac{1}{2} B r \right) \chi^{K'} = -(E - M + \frac{\alpha}{r}) \varphi^{K'} \\ \left(\frac{d}{dr} + \frac{i}{r} + \frac{1}{2} B r \right) \varphi^{K'} = (E + M + \frac{\alpha}{r}) \chi^{K'} \end{cases} \quad (3)$$

where $j = l + \frac{1}{2}$ is the total angular momentum quantum number and $M = m v_F^2 / E_0$. To get the eigenenergies and eigenfunctions, we decouple the two components in the same valley by substituting χ^τ into φ^τ . Then we get the second order differential equations for φ^τ from Eq.(2) and Eq.(3) as follows

$$\left[\left(\frac{\alpha}{r} + w_+ \right) \frac{d^2}{dr^2} + \frac{\alpha}{r^2} \frac{d}{dr} + \sum_{i=-3}^2 q_i r^i \right] \varphi^\tau = 0 \quad (4)$$

where $w_+ = E + W$ and q_i are as follows

$$\begin{cases} q_{-3} = \alpha^3 - j^2 \alpha \\ q_{-2} = \alpha^2 (3E + M) - (E + M)(j^2 - \tau j) \\ q_{-1} = \alpha (E + M)(3E - M) - \alpha \tau B (\tau j + 1) \\ q_0 = (E + M)[E^2 - M^2 - \tau B (\tau j + \frac{1}{2})] \\ q_1 = -\alpha B^2 / 4 \\ q_2 = -(E + M) B^2 / 4 \end{cases} \quad (5)$$

In the same way, we get the equations for χ^τ as

$$\left[\left(\frac{\alpha}{r} + w_- \right) \frac{d^2}{dr^2} + \frac{\alpha}{r^2} \frac{d}{dr} + \sum_{i=-3}^2 q_i r^i \right] \chi^\tau = 0 \quad (6)$$

where $w_- = E - W$ and q_i are

$$\begin{cases} q_{-3} = \alpha^3 - j^2 \alpha \\ q_{-2} = \alpha^2 (3E - M) - (E - M)(j^2 + \tau j) \\ q_{-1} = \alpha (E - M)(3E + M) + \alpha \tau B (-\tau j + 1) \\ q_0 = (E - M)[E^2 - M^2 + \tau B (-\tau j + \frac{1}{2})] \\ q_1 = -\alpha B^2 / 4 \\ q_2 = -(E - M) B^2 / 4 \end{cases} \quad (7)$$

We should point out that decoupling causes another regular singular point, i.e. $r = -\frac{\alpha}{E+M}$ for φ^τ and $r = -\frac{\alpha}{E-M}$ for χ^τ . In order to exclude these singular points from the positive axis, we will calculate only the energy levels above zero by solving φ^τ of Eq.(4) in this paper. The exact solution of such differential equations can be obtained from the series expansions around regular, irregular singular points and ordinary points, respectively.³¹

For Eq.(4), in regular region $0 \leq r < R_0$

$$\varphi^\tau = r^{\rho_j} \sum_{n=0}^{\infty} a_n r^n, \quad \rho_j = \sqrt{j^2 - \alpha^2}. \quad (8)$$

In irregular region $R_\infty < r < \infty$

$$\varphi^\tau = e^{-\frac{|B|r^2}{4}} r^v \sum_{n=0}^{\infty} b_n r^{-n}, \quad v = \frac{2q_0 - B w_+}{2B w_+}. \quad (9)$$

R_0 and R_∞ are chosen to ensure the proper behaviors of φ^τ in regular and irregular regions, respectively.

In ordinary point region $R_0 \leq r \leq R_\infty$, we divide it into k small sections $[r_i, r_{i+1}]$ where i is from 0 to $k-1$. The solution in each section is expanded around the center $r_i^c = \frac{r_i + r_{i+1}}{2}$ as

$$\varphi^\tau = C_i \sum_{n=0}^{\infty} c_n (r - r_i^c)^n + D_i \sum_{n=0}^{\infty} d_n (r - r_i^c)^n, \quad (10)$$

where $c_0 = 1, c_1 = 0, d_0 = 0, d_1 = 1$. In Eqs.(8),(9) and (10), a_n, b_n, c_n and $d_n (n > 0)$ are given by recurrence relations, and the eigenenergies and corresponding a_0, b_0, C_i, D_i (then the wave functions φ^τ and their partners χ^τ derived from Eq.(2) or Eq.(3)) are determined by the continuity condition. The method of series expansion

in different regions is a powerful tool to solve second order ordinary equations exactly whether they are derived from Dirac or Schrödinger equations.

Before we perform the numerical calculation, we discuss the analytical solutions in either Coulomb potential or magnetic field for the two valleys for further analysis.

In pure Coulomb potential, bound states only exist when $M \neq 0$. Make the transformation $j \rightarrow -j$ in Eq.(3) of valley K' and Eq.(3) becomes similar with Eq.2 of valley K . Thus $E_{C(n,j)}^{K'} = E_{C(n,-j)}^K$ and the energy levels of both valleys in pure Coulomb potential can be expressed as¹³

$$E_{C(n,j)}^\tau = \begin{cases} \frac{M(n+\sqrt{j^2-\alpha^2})}{\sqrt{(n+\sqrt{j^2-\alpha^2})^2+\alpha^2}} & \tau j > 0 \\ \frac{M(n+1+\sqrt{j^2-\alpha^2})}{\sqrt{(n+1+\sqrt{j^2-\alpha^2})^2+\alpha^2}} & \tau j < 0 \end{cases} \quad (11)$$

where $n = 0, 1, 2, \dots$ are the numbers of the nodes of the radial wave functions. In consideration of the valley degree of freedom, for $n = 0$, the energy levels are doubly degenerate, i.e, $E_{C(0,-|j|)}^{K'} = E_{C(0,|j|)}^K$ and for $n \geq 1$, they are quadruply degenerate, i.e, $E_{C(n,-|j|)}^{K'} = E_{C(n-1,|j|)}^{K'} = E_{C(n,|j|)}^K = E_{C(n-1,-|j|)}^K$. When $\alpha \ll 0.5$ (the critical value), expanding Eq.(11) in orders of α^4 , we acquire

$$E_{C(n,j)}^K - M = -\frac{M\alpha^2}{2N^2} + M\alpha^4\left(\frac{3}{8N^4} - \frac{1}{2|j|N^3}\right), \quad (12)$$

where $N = n + |l| + \frac{1}{2}$. Drop the last two terms and the familiar formula of two-dimensional hydrogen atom energy levels in non relativistic quantum mechanics are obtained.³¹ However this approximation fails as $\alpha \sim 0.5$.

In pure magnetic field, decouple the equations in each valley and four Schrödinger-like equations are obtained, which are analytic. The eigenenergies are the well known fourfold LLs

$$E_{L(n,l)}^\tau = \pm \sqrt{M^2 + 2\left[\frac{1}{2}(|l| + \tau l + 1 \pm 1) + n\right]B} \quad (13)$$

where the first “ \pm ” indicates the particle-hole symmetry in graphene, the second “ \pm ” represents the pseudospin of the sublattices A and B in graphene (for valley K , “+” (“-”) represents the sublattice A (B) and for valley K' , the signs are opposite) and $n = 0, 1, 2, \dots$ are the numbers of the nodes of the radial wave functions of the sublattice A (B). In the limit $M^2 \gg B$, suppose that the Dirac sea is filled and that the the sign of the pseudospin is “+” and then we obtain the LLs in nonrelativistic quantum mechanics

$$E_{L(n,l)}^K - M \approx \frac{1}{2M}(N+1)B \quad (14)$$

where $N = |l| + l + 2n$ is the index of LLs. The dependence on B - and \sqrt{B} - is the difference between non relativistic and relativistic quantum mechanics.

III. SPECTRA OF VALLEY K IN COULOMB AND MAGNETIC FIELDS

In this section, without loss of generality, we investigate how the spectra evolve with the mass, the Coulomb and the magnetic fields in valley K ($\tau = 1$) by the calculation method in Sec.II. Typically, we choose $\alpha = 0.3$ in the subcritical region and critical value $\alpha = 0.5$ of the Coulomb potential to investigate the effect of the Coulomb interaction. To understand the role of the mass, we consider the cases of $M = 0$ (massless) and $M = 10.524E_0$ (270 meV).^{9,23} In this paper, we only focus on the positive energy states when the Dirac sea is filled.³² We should point out that in the Coulomb and magnetic fields, the energy level ordering won't be dominated by either the Coulomb or the magnetic field. For each j (l), to distinguish the quantum states, we label the eigenstates of Eq.(4) as (n, j) ((n, l)) where $n = 0, 1, 2, \dots$ in the order of the increasing eigenenergies which lie above zero. In Tab.I, we give the energy levels when $M = 0, 10.524E_0$ and $\alpha = 0.3, 0.5$ at $B = 5T$. For convenience, the symbols a, b, c...therein labeling the quantum states $(0, \frac{1}{2})$, $(0, -\frac{1}{2})$, $(0, -\frac{3}{2})$, etc are adopted.

A. Spectra of massless Dirac electron

First we discuss the spectra of a massless electron. There are no bound states when $M = 0$ and $B = 0$. However, magnetic field helps to form bound states. From Tab.I, when $M = 0$ and $B = 5T$, the energy level of $\alpha = 0.3$ is higher than the corresponding level of $\alpha = 0.5$ and the level ordering doesn't change with α . Furthermore, in Fig.1(a) and (b), we give the first two LLs as functions of B for $\alpha = 0.3$ and 0.5 . We can see that the Coulomb interaction causes the LLs to split below. More specifically, $E_{(0,\frac{1}{2})(a)}^K < E_{(0,-\frac{1}{2})(b)}^K < E_{(0,-\frac{3}{2})(c)}^K < E_{(0,-\frac{5}{2})(d)}^K \dots$ fall below the first Landau level LL1 and $E_{(1,\frac{1}{2})(g)}^K < E_{(1,-\frac{1}{2})(h)}^K < E_{(0,\frac{3}{2})(m)}^K < E_{(1,-\frac{3}{2})(i)}^K < E_{(1,-\frac{5}{2})(j)}^K \dots$ fall below the second Landau level LL2. At $\alpha = 0.3$, the states g, h, m, i, j still stay above LL1, but at $\alpha = 0.5$, g falls even below LL1 and h is very close to LL1. Clearly, the smaller $\rho_j = \sqrt{j^2 - \alpha^2}$ in Eq.(8) is, the farther $E_{n,j}^K$ is away from the corresponding Landau level for ρ_j implies to what extent the Coulomb center attracts the electron. As a whole, the splitting of LLs increases with α and B , but the energies are still approximately proportional to \sqrt{B} , which characterizes the massless electron. When B , α and the quantum number n are fixed, the splitting between the states with the same ρ_j (e.g. b and a) is smaller than that between the states with $\rho_{-|j|-1}$ and with $\rho_{-|j|}$ (e.g. c and b). For the excited states with the same n , the splitting between the states with $\rho_{-|j|-1}$ and with $\rho_{-|j|}$ decrease with the increase of $|j|$. In Fig.3(a) and (c), we plot the radial distributions of the states a, b, g, h and m . The plot indicates that for the states with the same ρ_j and the same Landau level index N (e.g. a and b),

the state with $|j|$ (e.g. a) is more localized to the center than the state with $-|j|$ (e.g. b). That's why the state a (g) is below the state b (h). At the critical value $\alpha = 0.5$, the states a , b , g and h whose $\rho_j = 0$ are quite far away from their corresponding LLs and they will all disappear if $\alpha > 0.5$ because their ρ_j become imaginary. It means that the Coulomb potential is so strong that electrons with $|j| < \alpha$ collapse onto the Coulomb center, namely atomic collapse.¹⁵ Such phenomena will be continuing to take place with the increase of α . For example, the states c ($0, -\frac{3}{2}$) and m ($0, \frac{3}{2}$) will disappear when $\alpha > 1.5$, unless we properly regularize the Coulomb potential by taking into consideration the shape of the Coulomb center,²⁶ which is beyond the scope of the current paper.

B. Spectra of massive Dirac electron

We now move on to the massive case. From Tab.I, at $B = 5T$, the level orderings of $M = 10.524E_0$ are different from those of $M = 0$ and they change with α . Furthermore, in Fig.1(c) and (d), we give the first two LLs as functions of B when $\alpha = 0.3$ and 0.5 for $M = 10.524E_0$. It is shown that the energy level structures with respect to B are more complicated as bound states exist even without B . Take $\alpha = 0.3$ as an example. At weak magnetic field, the levels and their ordering are determined by the Coulomb interaction and the magnetic field serves as a perturbation to lift some degeneracies. Specifically, Fig.1(c) displays that $E_{(0, \frac{1}{2})(a)}^K < E_{(0, -\frac{1}{2})(b)}^K < E_{(1, \frac{1}{2})(g)}^K < E_{(0, \frac{3}{2})(m)}^K < E_{(0, -\frac{3}{2})(c)}^K < E_{(1, -\frac{1}{2})(h)}^K < E_{(0, -\frac{5}{2})(d)}^K < \dots$ at $B = 0.1T$. The degenerate states $(n, -|j|)$ and $(n+1, |j|)$ such as the states b and g in pure Coulomb field (see Eq.(11)) are lifted by B . As B increases, the states h , m and g which are below LL1 at weak magnetic field will climb above LL1 in sequence and at high magnetic fields the level ordering will become more like that of the massless case (Fig.1(a)). Along with the transition of the level ordering, crossing of levels happen. In Fig.1(c), the state m (g) intersects with the state c at about $1.3T$ ($3.3T$). As the ground state a is most influenced by the Coulomb interaction, it remains well below the gap ($10.524E_0$) even at high magnetic fields while the other states climb over the gap in sequence as the magnetic field increases. From the viewpoint of the LLs, their degeneracies are all lifted by the Coulomb field and they split into quasi linear lines, i.e. $\propto B$, different from the quasi square root dependence on B of the massless case. At the critical value $\alpha = 0.5$, the splitting of the LLs is more clear and the spacing is larger. The state h (m) intersects with the state c at a higher magnetic field $2.5T$ ($4.0T$), but the state g stays below the state c . Especially, from Eq.(11), for $\alpha = 0.5$, with $E_{C(0, \frac{1}{2})(a)}^K = 0$, the state a with its $\rho_j = 0$ is at the point of atomic collapse and the maximum of its eigenenergy is only $0.23E_0$ at $10T$, much smaller than LL1. From the above analysis, it is evident that the massive spectra are quite different from the massless spectra, especially

the respective quasi B - and quasi \sqrt{B} - dependence of the energy levels and the variation of energy level ordering in the massive case. The results will be helpful in understanding the electronic structure of planar Dirac electron in QED.

C. Binding energy

To understand how the contribution of the Coulomb interaction to the variation of $E_{n,j}^K$, we define the binding energy as the difference of the LLs and the energy

$$E_{B(n,j)}^K = E_{L(n,j)}^K - E_{n,j}^K \quad (15)$$

where we adopt $E_{L(n,j)}^K$ in Eq.(13) above zero. In Fig.2(a) we give the binding energies of Dirac electron as functions of mass with $\alpha = 0.3$ and $B = 10T$. The evolutions of the binding energies with the mass vary with the total angular momentum quantum number j . For the states with $j > 0$ (e.g. a, m, n), their binding energies increase with the mass, but for the states with $j < 0$ (e.g. b, c, d), their binding energies decrease with the mass except that the state b experiences a minimum at $M \approx 7.8E_0$ and then increases slowly. Interestingly, the binding energies of the states b and m (c and n , d and o) with the same $|l|$ ($l = j - \frac{1}{2}$) tend towards the same limit when M is large enough. In Fig.3, we plot the radial distributions of $\Psi_{(0, \pm \frac{1}{2})}^K$, $\Psi_{(1, \pm \frac{1}{2})}^K$ and $\Psi_{(0, \frac{3}{2})}^K$ for $\alpha = 0.3$ and $B = 10T$ with $M = 0, 10.524E_0$. From Fig.3(a) and (c), We can see that for $M = 0$, both the upper and lower components of the state b are closer than those of the state m , causing, causing $E_{B(0, -\frac{1}{2})(b)}^K$ larger than $E_{B(0, \frac{3}{2})(m)}^K$. From Fig.3(b) and (d), for $M = 10.524E_0$, the lower components of the states b and m become smaller and their upper components become more similar, so the difference between $E_{B(0, -\frac{1}{2})(b)}^K$ and $E_{B(0, \frac{3}{2})(m)}^K$ decreases.

To investigate how the binding energies evolve with the magnetic field, in Fig.2(b) we plot the binding energies of the states a, b, c, m, n as functions of B with $\alpha = 0.3$ with $M = 0, 10.524E_0$. They all increase with B for the magnetic field drives the electron to the Coulomb center. For $M = 0$, their binding energies approach zero as B approaches zero for no bound states exist for $M = 0$ and $B = 0$. For $M = 10.524E_0$, their binding energies approach certain values as B approaches zero for bound states exist for $M \neq 0$ and $B = 0$. As B increases, the binding energies of the states with $j > 0$ of the massless case grow faster than those of the massive case and will exceed those of the massive case at certain magnetic field, but for the states with $j < 0$ (e.g. m, n), their binding energies of the massless case remain below those of the massive case. The different dependence of the binding energies on the mass and the magnetic field helps to distinguish the massless and the massive Dirac electron.

What is mentioned above clearly shows that the planar Dirac electronic states can be controlled by the mass, Coulomb and magnetic fields. The j -, α - and M -

dependent quantum behaviors can be helpful in making devices based on graphene and in experimental designs such as Landau level spectroscopy or scanning tunneling microscopy (STM) in graphene.³³

IV. VALLEY SPLITTING AND INTER-VALLEY MIXING IN COULOMB AND MAGNETIC FIELDS

The difference between QED and graphene is that valley splitting and inter-valley mixing of K and K' have to be taken into account when the valley degeneracy is broken and inter-valley coupling is nonnegligible. In what follows, we will focus the valley splitting and inter-valley mixing in graphene based on the effective mass theory.

A. Valley splitting

Before we discuss the valley splitting of K and K' in this section, we mention that the valley degeneracy can't be broken by magnetic field unless $M \neq 0$. When $M = 0$, make the transformation of $\varphi^{K'} \leftrightarrow -\chi^{K'}$ in Eq.(3) of valley K' and they become the same as Eq.(2) of valley K . Thus, $E_{n,j}^{K'} = E_{n,j}^K$ for $M = 0$. Therefore, we only need to investigate the valley splitting in the case of $M \neq 0$.

We choose $M = 10.524E_0$ and $\alpha = 0.1, 0.3$ to see how the spectra of valley K' evolve with the magnetic field. In Fig.4, we give the spectra of valley K' along with some energy levels of K for comparison. Clearly, it is observed that the degenerate $E_{n,-j}^{K'}$ and $E_{n,j}^K$ in Eq.(11) are lifted by the magnetic field. The valley splitting results from the breaking of the true time-reversal symmetry by the magnetic field and the breaking of the effective time-reversal symmetry by the mass.³⁴ As the full spectra of K and K' are complicated, we will only turn to the splitting of the ground and first excited states for $\alpha = 0.1, 0.3$, respectively. When $\alpha = 0.1$, it is clear that the state B of valley K' is always the ground state. However, the first excited state transfers from the state a of valley K to the state C of valley K' at $B \approx 2T$. The largest splitting spacing is about $\Delta^{KK'} \approx 0.19E_0 = 4.87meV$ at $B \approx 2T$. For $\alpha = 0.3$, the state B of valley K' is still the ground state and in the range of $0 \sim 10T$ of the magnetic field, the state a of valley K is the first excited state. The splitting between the states B and a increases linearly with B . The splitting reaches $\Delta^{KK'} \approx 0.86E_0 = 22.06meV$ at $B = 10T$.

Finally, it is worthwhile to point out that the splitting of valleys K and K' is of particular importance in experiments and the design of electronic devices based on graphene.^{35,36} The breaking of the valley degeneracy provides a way to observe the intrinsic physics of a single valley in experiments. The low-lying states of Dirac electron can be tuned between valley K and valley K' by adjusting B , α and M in the subcritical region

$\alpha < 0.5$ which may be useful in the manipulation of the valleys in graphene.³⁶

B. Inter-valley mixing

In this section, we discuss how the Coulomb field affects the inter-valley mixing in graphene. For the Coulomb field $\frac{1}{r}$, its three dimensional Fourier transformation is $\frac{1}{q^2}$ and it is often treated as a long-range field which doesn't involve inter-valley mixing in semiconductors.³⁷ However, its two dimensional Fourier expansion in graphene is $\frac{1}{q}$,¹⁴ less singular than $\frac{1}{q^2}$. Therefore, we have to carefully examine the inter-valley mixing caused by the Coulomb impurity in graphene.^{14,19,26} Based on the effective mass theory, Ando and Nakanishi³⁸ presented an effective way to estimate the coupling strength of the two valleys by the equation

$$U'_{A(B)}(R) = \sum_{R'_{A(B)}} g(R - R'_{A(B)}) e^{i(\vec{K}' - \vec{K}) \cdot \vec{R}'_{A(B)}} U_{A(B)}(R'_{A(B)}) \quad (16)$$

where $U'_{A(B)}(R)$ is the coupling strength between the $A(B)$ sublattices of K and K' , $U_{A(B)}(R'_{A(B)})$ is the on-site energy and $g(R)$ normalized by $\sum_R g(R) = 1$ has an appreciable amplitude in the region where $|R|$ is smaller than a few times of the lattice constant and decays rapidly with increasing $|R|$.³⁸ For the potentials whose ranges are shorter than the lattice constant, $U_{A(B)}(R'_{A(B)})$ may be treated as a delta function and thus the coupling strength $U'_{A(B)}(R)$ is also a delta function.³⁸ For the potentials that vary slowly on the scale of the lattice constant, the phase $e^{i(\vec{K}' - \vec{K}) \cdot \vec{R}'_{A(B)}}$ in Eq.(16) leads to the coupling strength $U'_{A(B)}(R) = 0$.^{38,40} As the Coulomb potential contains both long-ranged and short-ranged portions, it is difficult for us to evaluate the coupling strength quantitatively directly from Eq.(16). Recently Zhang et al³⁹ have estimated the matrix elements between the two valleys of graphene under periodic external potentials as

$$U_{KK'} = \langle \Psi^K | e^{-i(\vec{K} - \vec{K}') \cdot \vec{r}} U(r) | \Psi^{K'} \rangle \quad (17)$$

where $U(r)$ is the external potentials and their results were in agreement with those acquired by the density function theory. Actually, the integral kernel $e^{-i(\vec{K} - \vec{K}') \cdot \vec{r}} U(r)$ in Eq.(17) is the result derived from Eq.(16) by supposing $g(R)$ behaves like the delta function.

Based on Ref.38 and Ref.39, we estimate the matrix elements between K and K' caused by the Coulomb po-

tential as

$$\begin{aligned}
U_{KK'} &= \langle \Psi_{n,j}^K | e^{-i(\vec{K}-\vec{K}')\cdot\vec{r}} U(r) | \Psi_{n',j'}^{K'} \rangle \\
&= -\alpha \frac{i}{2\pi} \int_0^{2\pi} \int_0^\infty \frac{1}{r} [\varphi_{n,j}^K \varphi_{n',j'}^{K'} e^{i(j'-j+1)\theta} - \\
&\quad \chi_{n,j}^K \chi_{n',j'}^{K'} e^{i(j'-j-1)\theta}] e^{-i(\vec{K}-\vec{K}')\cdot\vec{r}} dr d\theta \quad (18)
\end{aligned}$$

where $U(r) = -\frac{\alpha}{r}$. In order to calculate the inter-valley mixing of the lowest lying states, we limit the quantum states (n, j) to $0 \leq n \leq 3$ and $-\frac{5}{2} \leq j \leq \frac{7}{2}$ in each valley. In the direct sum spaces of the two valleys, we acquire the spectra in consideration of inter-valley mixing by exact diagonalization.

In Fig.5 we plot the spectra of the two lowest lying states with and without inter-valley mixing as functions of the magnetic field for $\alpha = 0.3, 0.4$ and $M = 0, 10.524E_0$. For the massless case ($M = 0$), the degenerate states $(K, 0, \frac{1}{2})$ and $(K', 0, \frac{1}{2})$ without inter-valley mixing are lifted by the inter-valley mixing and the splitting increases with the magnetic field. In Fig.5(a), for $\alpha = 0.3$, the difference between the energies with and without inter-valley mixing is not remarkable, about 2% at $B = 10T$. In Fig.5(b), for $\alpha = 0.4$, the difference becomes larger, about 6% at $B = 10T$. For the massive case ($M = 10.524E_0$), the spacing between the two lowest states with inter-valley mixing is larger than that between the two ground states of K and K' without inter-valley mixing and the spacing changes little with the magnetic field. In Fig.5(c), for $\alpha = 0.3$, the difference between the energies with and without inter-valley mixing is still tolerable, about 8% at $B = 1T$, which is larger than the massless case. The wave functions of the massive electron are more localized and their upper components are larger than the lower components (see Fig.3), causing the matrix elements of the massive electron in Eq.(18) larger than those of the massless electron. However, in Fig.5(d), for $\alpha = 0.4$ near the critical value 0.5 and $B = 1T$, the ground energy level without inter-valley mixing is 160% of the first energy level with inter-valley mixing, indicating that the electron is so localized by the Coulomb field and the inter-valley is so strong that the effective mass theory breaks down.

Our calculation shows that the inter-valley mixing increases with the strength of the Coulomb potential, especially for the massive case. When the Coulomb strength $\alpha \leq 0.3$, the inter-valley mixing is not remarkable (less than 10%), especially for the massless electron and the effective mass theory can still be considered valid. However, near the critical value $\alpha = 0.5$, the electron is so localized to the Coulomb center that the inter-valley mixing can't be neglected, where the effective mass theory in graphene breaks down.

V. CONCLUSION

In summary, by the series expansion method, we have acquired the exact energies of both ground and excited

states of the planar Dirac electron in Coulomb and magnetic fields and our method may promote exact solutions of Dirac equation in other complex electromagnetic fields in QED. In graphene, we calculate and analyze the spectra of the valley K in detail to reveal the competition between the Coulomb and the magnetic fields. The energy levels and their ordering can be controlled by the mass, the Coulomb and magnetic fields in graphene. The different characteristics between the massless and massive Dirac electrons are reflected in their binding energies.

As graphene has K and K' valleys, we investigate the valley splitting and inter-valley mixing by the calculation method developed in this paper. The valley degree of freedom and the splitting spacings in graphene can be tuned by the mass, Coulomb and magnetic fields. By exact diagonalization, we estimate the inter-valley mixing caused by the Coulomb field and find that the inter-valley mixing depends on the strength of the Coulomb field. When the strength of the Coulomb field is near the critical value $\alpha = 0.5$, the effective mass theory in graphene breaks down. We hope our calculations may contribute to future experiment designs.

Financial supports from NSF China (Grant No. 10974108 and 11174170) and the "973" Programme of China (No. 2011CB921901) are gratefully acknowledged.

- * Electronic address: zjl-dmp@tsinghua.edu.cn
- ¹ K. S. Novoselov, A. K. Geim, S. V. Morozov, D. Jiang, Y. Zhang, S. V. Dubonos, I. V. Grigorieva, and A. A. Firsov, *Science* **306**,666 (2004).
 - ² K. S. Novoselov, A. K. Geim, S.V. Morozov, D. Jiang, M. I. Katsnelson, I.V. Grigorieva, S.V. Dubonos, and A. A. Firsov, *Nature (London)* **438**, 197 (2005).
 - ³ Yuanbo Zhang, Yan-Wen Tan, Horst L. Stormer, and Philip Kim, *Nature (London)* **438**, 201 (2005).
 - ⁴ A. H. Castro Neto, F. Guinea, N. M. R. Peres, K. S. Novoselov and A. K. Geim, *Rev. Mod. Phys.* **81**, 109 (2009).
 - ⁵ G. W. Semenoff, *Phys. Rev. Lett.* **53**, 2449 (1984).
 - ⁶ S. Y. Zhou, G.-H. Gweon, A. V. Fedorov, P. N. First, W. A. De Heer, D.-H. Lee, F. Guinea, A. H. Castro Neto and A. Lanzara, *Nat Mater.* **6**, 770 (2007).
 - ⁷ C. L. Kane and E. J. Mele, *Phys. Rev. Lett.* **95**, 226801 (2005).
 - ⁸ D. Haberer, D. V. Vyalikh, S. Taioli, B. Dora, M. Farjam, J. Fink, D. Marchenko, T. Pichler, K. Ziegler, S. Simonucci, M. S. Dresselhaus, M. Knupfer, B. Büchner, and A. Grüneis, *Nano. Lett.* **10**, 3360 (2010).
 - ⁹ J.-H.Chen, C. Jang, S. Adam, M. S. Fuhrer, E. D. Williams and M.Ishigami, *Nat Phys.* **4**, 377 (2008).
 - ¹⁰ E.H.Hwang, S.Adam, and S.Das Sarma, *Phys. Rev. Lett.* **98**, 186806 (2007).
 - ¹¹ Kentaro Nomura and A. H. MacDonald. **98**, 076602 (2007).
 - ¹² T.Stauber, N.M.R.Peres,and F.Guinea, *Phys. Rev. B* **76**, 205423 (2007).
 - ¹³ D. S. Novikov, *Phys. Rev. B* **76**, 245435 (2007).
 - ¹⁴ Vitor M. Pereira, Johan Nilsson, and A. H. Castro Neto, *Phys. Rev. Lett.* **99**, 166802 (2007).
 - ¹⁵ A.V. Shytov, M. I. Katsnelson, and L. S. Levitov, *Phys. Rev. Lett.* **99**, 236801 (2007).
 - ¹⁶ Vitor M. Pereira, Valeri N. Kotov, and A. H. Castro Neto, *Phys. Rev. B* **78**, 085101 (2008).
 - ¹⁷ Ivan S.Terekhov, Alexander I.Milstein, Valeri N.Kotov, and Oleg P.Sushkov, *Phys. Rev. Lett.* **100**, 076803 (2008).
 - ¹⁸ M. M. Fogler, D. S. Novikov, and B. I. Shklovskii, *Phys. Rev. B* **76**, 233402 (2007).
 - ¹⁹ Wei Zhu, Zhengfei Wang, Qinwei Shi, K.Y.Szeto, Jie Chen, and J.G.Hou, *Phys. Rev. B* **79**, 155430 (2009).
 - ²⁰ M. L. Sadowski, G. Martinez, and M. Potemski, C. Berger and W. A. de Heer, *Phys. Rev. Lett.* **97**, 266405 (2006).
 - ²¹ P. Neugebauer, M. Orlita, C. Faugeras, A.-L. Barra, and M. Potemski, *Phys. Rev. Lett.* **103**, 136403 (2009).
 - ²² Choon-Lin Ho and V. R. Khalilov, *Phys. Rev. A* **61**, 032104 (2000).
 - ²³ B.S. Kandemira and A. Mogulkoc, *Eur. Phys. J. B.* **74**, 535 (2010).
 - ²⁴ Y. Zhang,Z. Jiang, J.P.Small, M.S.Purewal, Y.-W.Tan, M.Fazlollahi, J.D.Chudow, J.A.Jaszczak, H.L.Stormer, and P.Kim, *Phys. Rev. Lett.* **96**, 136806 (2006).
 - ²⁵ M.Koshino and T. Ando , *Phys. Rev. B* **75**, 033412 (2007).
 - ²⁶ A. L. C. Pereira and P. A. Schulz, *Phys. Rev. B* **77**, 075416 (2008).
 - ²⁷ J. M. Pereira, F. M. Peeters, R. N. Costa Fil- ho. and G. A. Farias, *J. Phys.: Condens. Matter* **21**, 045301 (2009).
 - ²⁸ P. Recher, B. Trauzettel, A. Rycerz, Ya. M. Blanter, C. W. J. Beenakker, and A. F. Morpurgo, *Phys. Rev. B* **76**, 235404 (2007).
 - ²⁹ K.Nomura and A.H.MacDonald, *Phys. Rev. Lett.* **96**,256602(2006)
 - ³⁰ N. Shibata and K. Nomura, *Phys. Rev. B* **77**, 235426 (2008).
 - ³¹ Jia-Lin Zhu, *Phys. Rev. B* **39**, 8780 (1989).
 - ³² Wolfgang Häusler, and Reinhold Egger, *Phys. Rev. B* **80**, 161402 (2009).
 - ³³ Victor W.Brar, Régis Decker, Hans-Michael Solowan, YangWang, Lorenzo Maserati, Kevin T.Chan, Hoonkyung Lee, Çağlar O.Girit, Alex Zettl, Steven G. Louie, Marvin L. Cohen and Michael F.Crommie, *Nat Phys.* **7**, 43 (2011).
 - ³⁴ Patrik Recher, Johan Nilsson, Guido Burkard and Björn Trauzettel, *Phys. Rev. B* **79**, 085407 (2009).
 - ³⁵ A.Rycerz, J.Tworzyd and C.W.J.Beenakker, *Nat Phys.* **3**, 172 (2007).
 - ³⁶ Patrik Recher and Björn Trauzettel, *Nanotechnology.* **21**, 302001 (2010).
 - ³⁷ Sokrates T. Pantelides, *Rev. Mod. Phys.* **50**, 797 (1978).
 - ³⁸ Tsuneya Ando and Takeshi Nakanishi, *J.Phys.Soc.Jpn.* **67**, 1704 (1998).
 - ³⁹ Aihua Zhang, Zhenxiang Dai, Lei Shi, Yuan Ping Feng, and Chun Zhang, *J.Chem.Phys.* **133**, 224705 (2010)
 - ⁴⁰ C. W. J. Beenakker, *Rev. Mod. Phys.* **80**, 1337 (2008).

Figures

FIG. 1: Valley K : Energy spectra of Dirac electron as functions of B for $M = 0$ with $\alpha = 0.3$ (a) and 0.5 (b) and $M = 10.524E_0$ with $\alpha = 0.3$ (c) and 0.5 (d), respectively. The solid and dashed lines label the first and second LLs in the presence of the Coulomb potential, respectively. The lines labeled with LL1 and LL2 are the first and second Landau levels without the Coulomb potential. The energy level symbols are in accordance with Tab.I.

FIG. 2: Valley K : (a) Binding energies of states $(0, \pm\frac{1}{2}), (0, \pm\frac{3}{2}), (0, \pm\frac{5}{2})$ and $(0, \frac{7}{2})$ as functions of M for $\alpha = 0.3$ with $B = 10T$. (b) Binding energies of states $(0, \pm\frac{1}{2}), (0, \pm\frac{3}{2})$ and $(0, \frac{5}{2})$ as functions of B for $\alpha = 0.3$ with $M = 0$ (solid lines) and $10.524E_0$ (dashed lines). The symbols of the states are in accordance with Tab.I.

FIG. 3: The radial wave functions of the valley K for the states $(0, \pm\frac{1}{2}), (1, \pm\frac{1}{2}), (0, \frac{3}{2})$: the upper components φ for $M = 0$ (a) and $M = 10.524E_0$ (b) and the lower components χ for $M = 0$ (c) and $M = 10.524E_0$ (d) at $\alpha = 0.3$ and $B = 10T$. φ and χ are normalized by $\int_0^\infty |\varphi|^2 + |\chi|^2 dr = 1$. The symbols of states are in accordance with Tab.I.

FIG. 4: Valleys K and K' : Energy spectra of Dirac electron in Coulomb and magnetic fields as functions of B for $M = 10.524E_0$ with $\alpha = 0.1$ (a) and 0.3 (b). The symbols of states are in accordance with Tab.I. The capital letters represent the states of K' and the lower-case letters the states of K .

FIG. 5: Inter-valley mixing: The two lowest lying states (solid lines) as functions of B in consideration of the inter-valley mixing. The parameters of the Coulomb field and the mass are (a) $\alpha = 0.3, M = 0$, (b) $\alpha = 0.4, M = 0$, (c) $\alpha = 0.3, M = 10.524E_0$, (d) $\alpha = 0.4, M = 10.524E_0$. The dashed lines represent the ground states of valleys K and K' without inter-valley mixing for comparison.

Tables

TABLE I: Energy levels of Dirac electronic states when $M = 0, 10.524E_0$ and $\alpha = 0.3, 0.5$ in the case of $B = 5T$. For convenience, a, b, c, d... are adopted to label the level ordering. The energies are expressed in the unit E_0 .

(n, j)	$M = 0$		$M = 10.524E_0$	
	$\alpha = 0.3$	$\alpha = 0.5$	$\alpha = 0.3$	$\alpha = 0.5$
a: $(0, \frac{1}{2})$	(a)2.3883	(a)1.1006	(a)8.6387	(a)0.1180
b: $(0, -\frac{1}{2})$	(b)2.5442	(b)1.5811	(b)10.4460	(b)9.4519
c: $(0, -\frac{3}{2})$	(c)2.8062	(c)2.5496	(c)10.6445	(g)9.6757
d: $(0, -\frac{5}{2})$	(d)2.8803	(d)2.6849	(d)10.7127	(c)10.3736
e: $(0, -\frac{7}{2})$	(e)2.9208	(e)2.7558	(g)10.7241	(m)10.4468
f: $(0, -\frac{9}{2})$	(f)2.9474	(f)2.8018	(e)10.7512	(h)10.4712
g: $(1, \frac{1}{2})$	(g)3.8869	(g)3.0596	(f)10.7769	(d)10.5120
h: $(1, -\frac{1}{2})$	(h)3.9442	(h)3.1832	(m)10.9311	(e)10.5838
i: $(1, -\frac{3}{2})$	(m)4.0837	(m)3.7970	(h)10.9976	(f)10.6299
j: $(1, -\frac{5}{2})$	(i)4.1459	(i)3.9092	(i)11.1249	(i)10.8924
k: $(1, -\frac{7}{2})$	(j)4.2073	(j)4.0228	(j)11.1776	(j)10.9938
l: $(1, -\frac{9}{2})$	(k)4.2423	(k)4.0845	(k)11.2097	(k)11.0523
m: $(0, \frac{3}{2})$	(l)4.2659	(l)4.1255	(l)11.2319	(l)11.0918
n: $(0, \frac{5}{2})$	(n)5.1790	(n)4.9688	(n)11.5248	(n)11.2607
o: $(0, \frac{7}{2})$	(o)6.0727	(o)5.8983	(o)12.0047	(o)11.8054

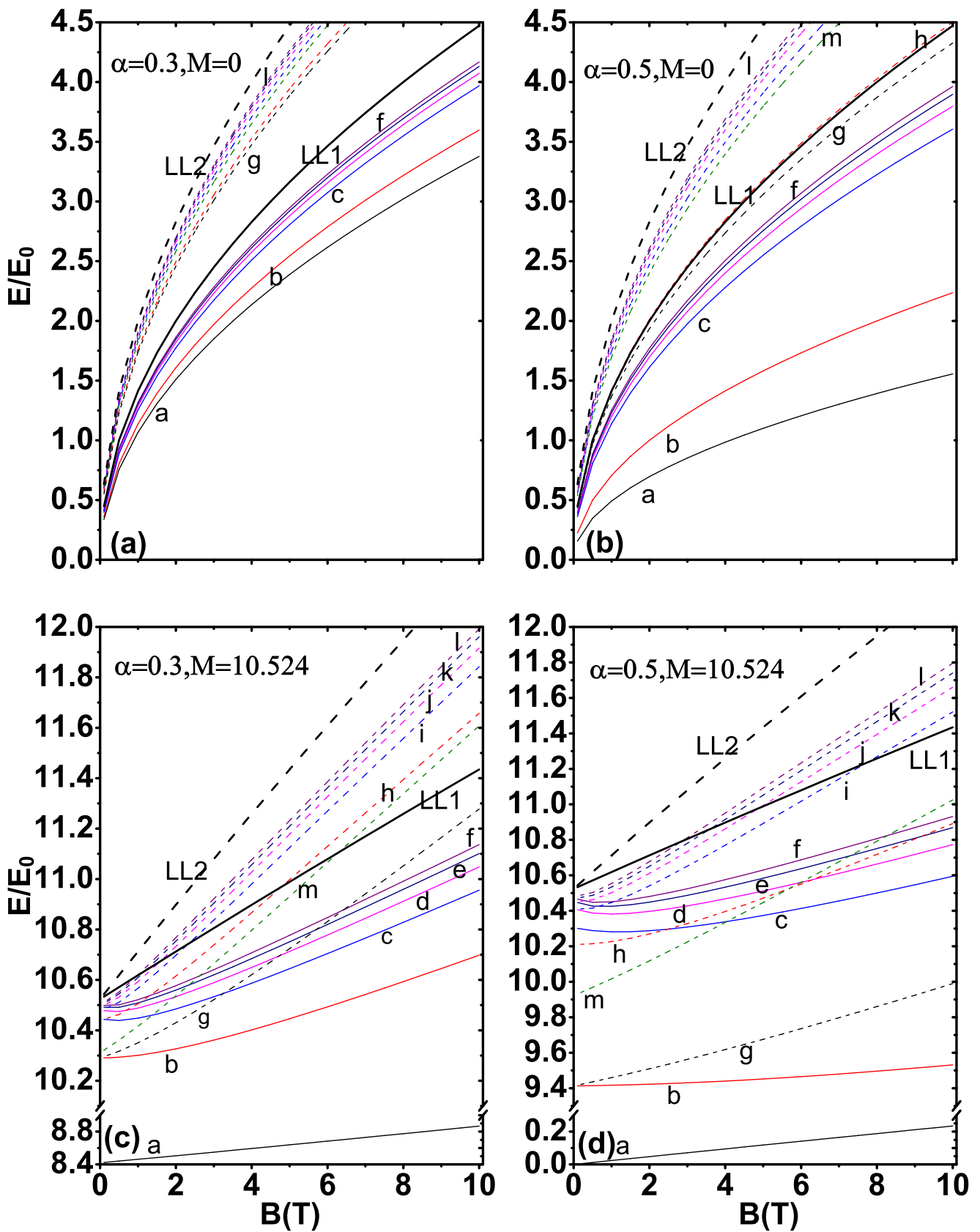


Figure 1

LA13261B

18Nov2011

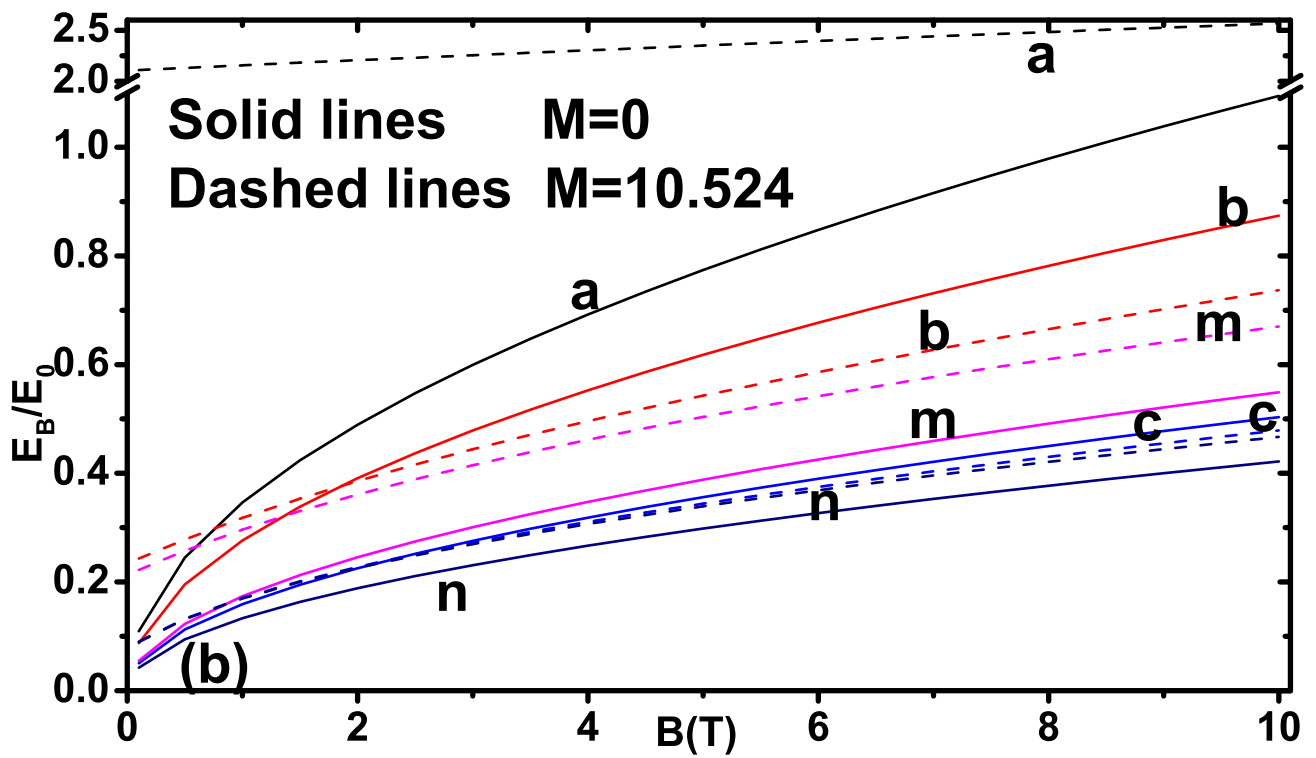
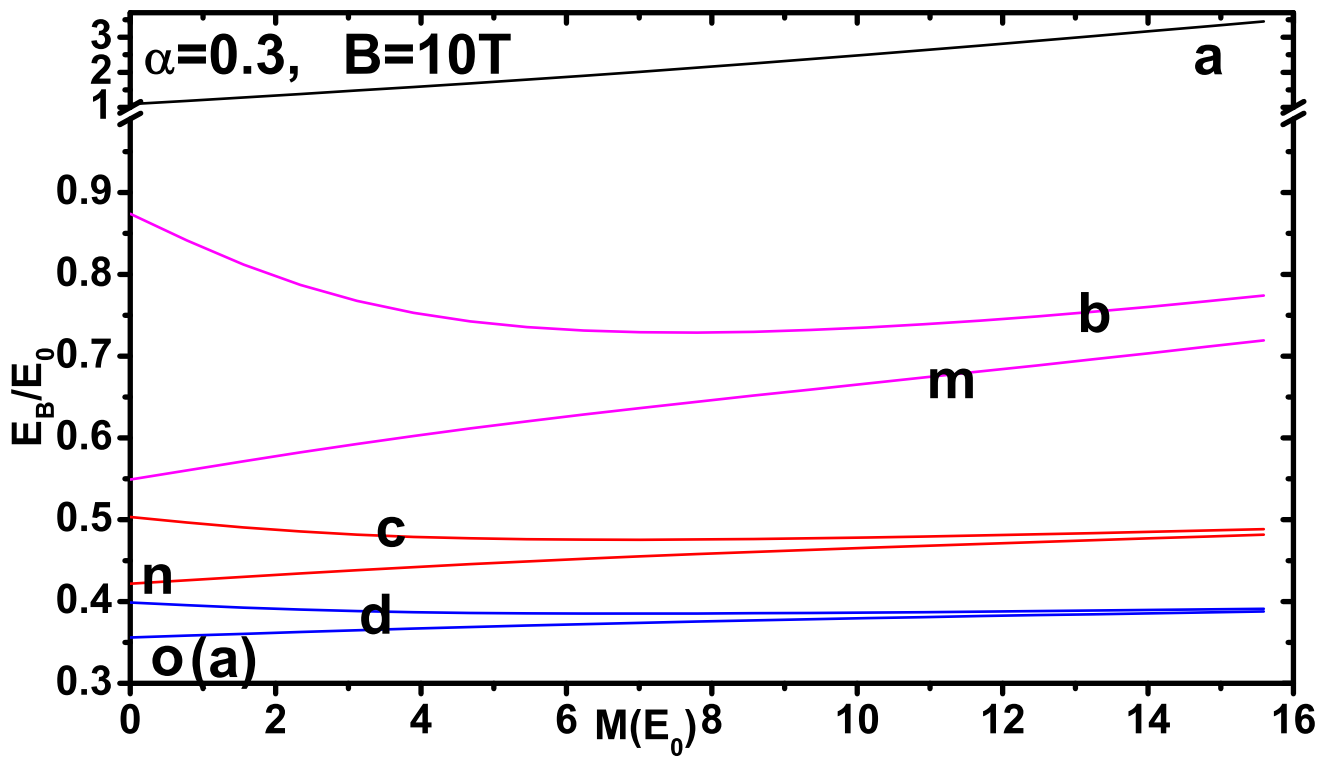


Figure 2

LA13261B

18Nov2011

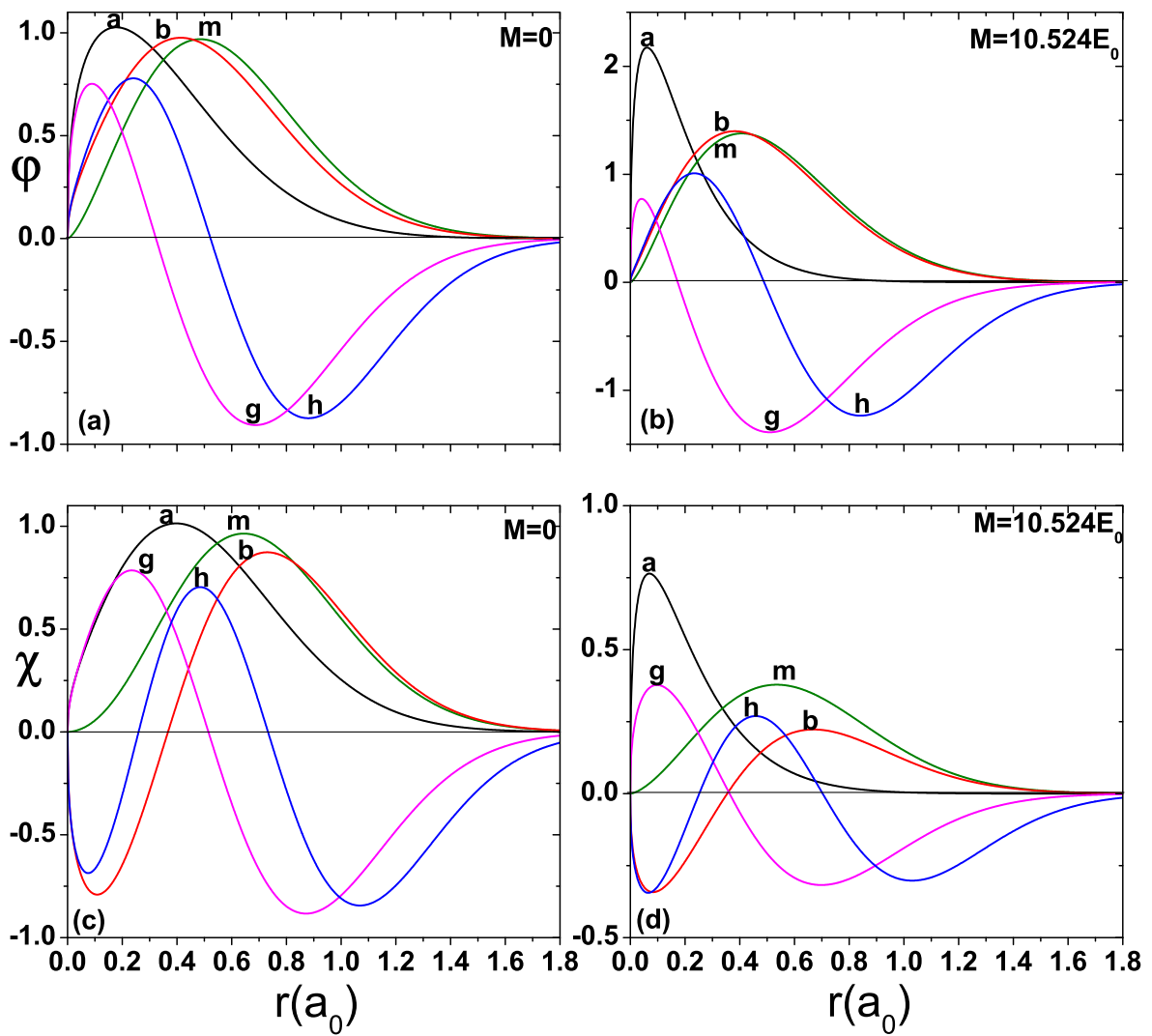


Figure 3 LA13261B 18Nov2011

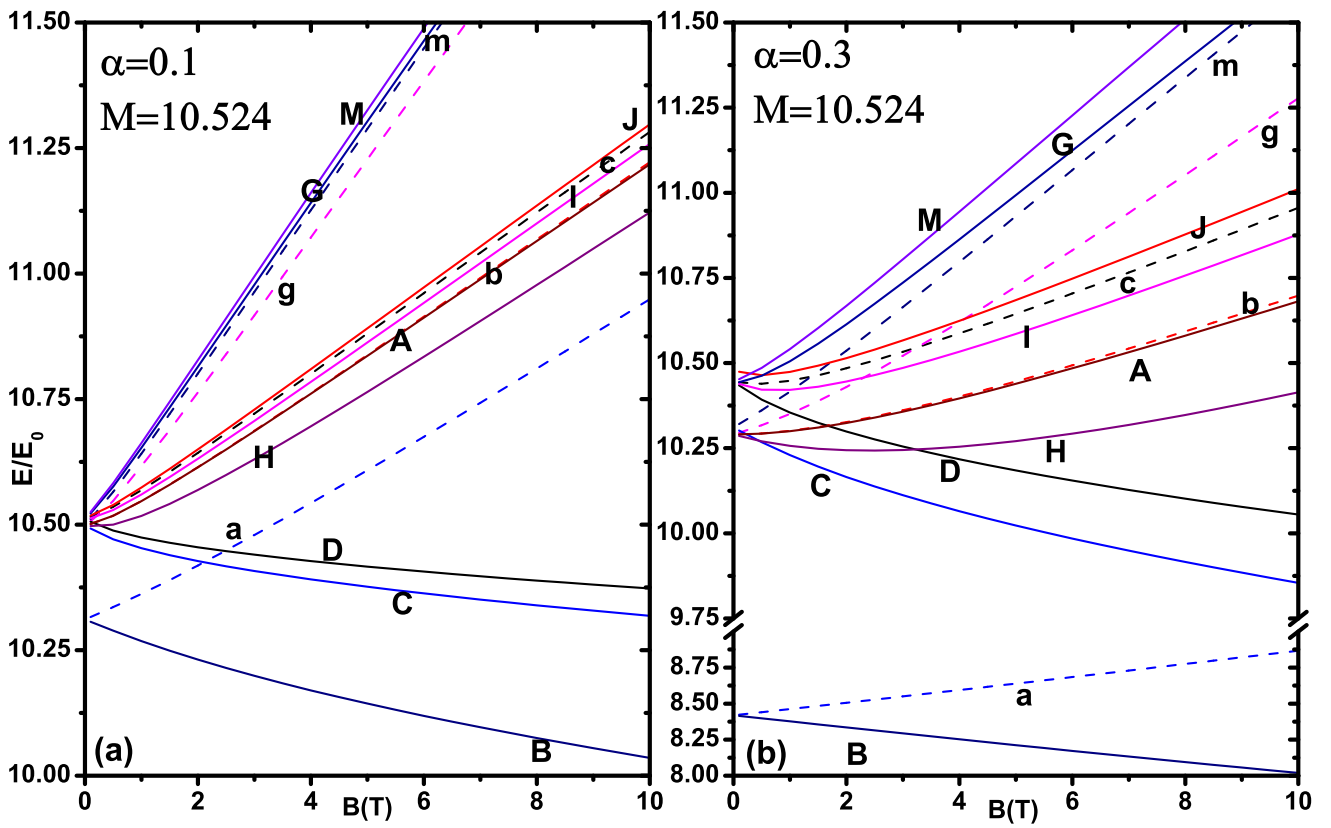


Figure 4 LA13261B 18Nov2011

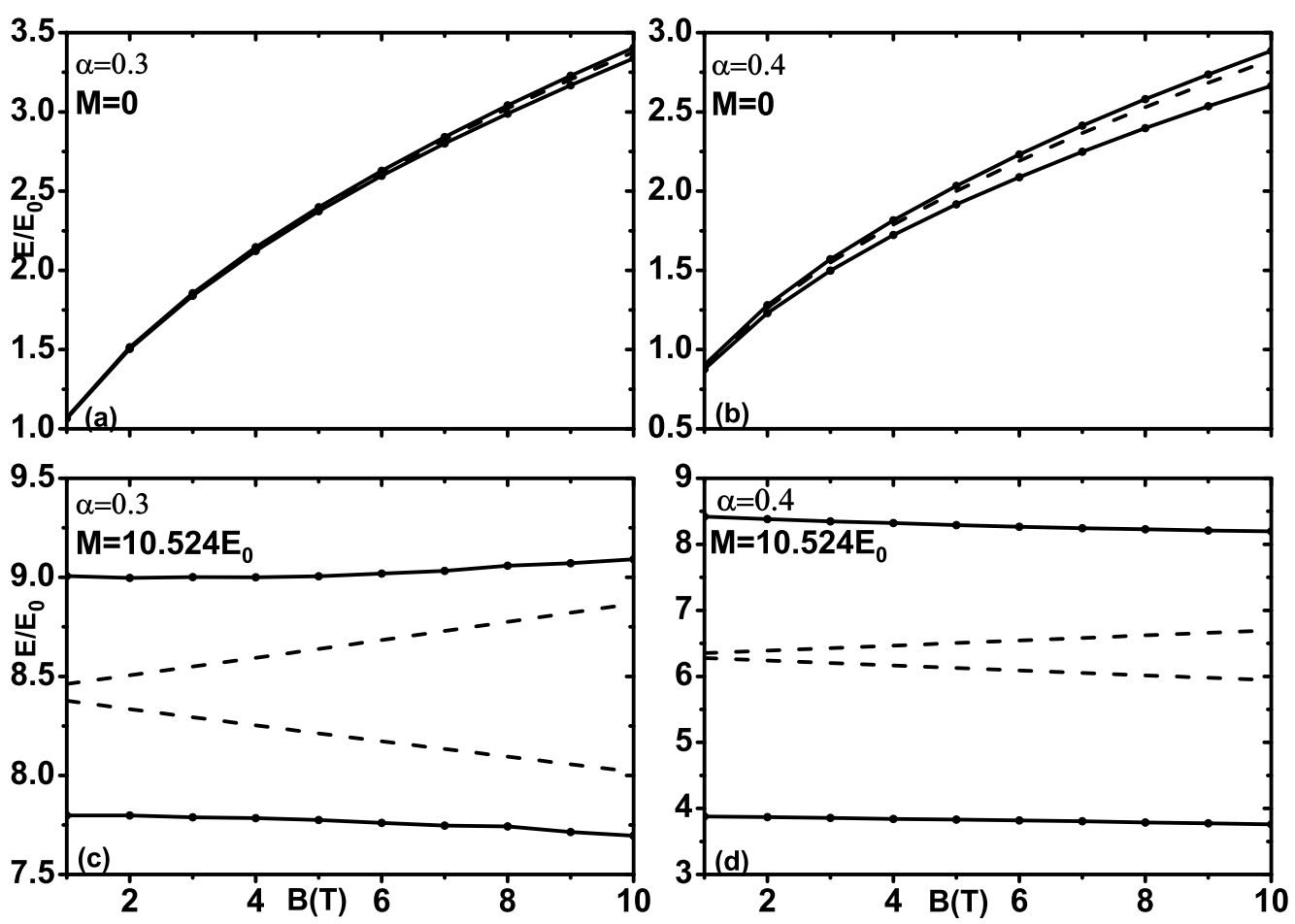


Figure 5

LA13261B

18Nov2011